Spark Plasma Sintering of PSZ-Ti Composites Using Ceramic-Coated Ti Powder to Suppress Sintering Reactions

Spark plasma sintering of PSZ-Ti composites using ceramic-coated Ti powder to suppress sintering reactions

Tomoyuki Fujii[*1], Masaki Suzuki[2], Keiichiro Tohgo[3], and Yoshinobu Shimamura[4]

[1] fujii.tomoyuki@shizuoka.ac.jp, Department of Mechanical Engineering, Shizuoka University, 3-5-1, Johoku, Naka-ku, Hamamatsu 432-8561, Japan

[2] suzuki.masaki.14@shizuoka.ac.jp, Department of Mechanical Engineering, Shizuoka University

[3] tohgo.keiichiro@shizuoka.ac.jp, Department of Mechanical Engineering, Shizuoka University

[4] shimamura.yoshinobu@shizuoka.ac.jp, Department of Mechanical Engineering, Shizuoka University

[*] **Corresponding author: Dr. T. Fujii**

E-mail: fujii.tomoyuki@shizuoka.ac.jp

Tel & Fax: +81-53-478-1029

Abstract

This study aims to fabricate partially stabilized zirconia (PSZ)-titanium (Ti) composites to produce implants having ceramic and metallic characteristics. To fabricate such materials via powder metallurgy, sintering reactions must be suppressed. In this study, ceramic-coated Ti powder was used as a starting material to suppress Ti oxide formation. Yttria was coated on Ti powder using the sol-gel technique, the Ti powder was mixed with PSZ powder, and the mixed powders were sintered. From the results of optical microscopy and XRD analysis, dense PSZ-Ti composites containing the yttria phase were successfully fabricated without any reaction products. Hardness and bend tests revealed that the hardness and elastic modulus of the composites increased with the increase of PSZ content and agreed with the predicted values based on the rule of mixtures. Bend tests also revealed that the strength did not improve, as the brittle yttria phase preferentially fractured in the composites subjected to bending.

Keywords: Sintering; Composite materials; Sol-gel processes, Coating materials, Mechanical properties

1. Introduction

Biomaterials have been developed for medical applications such as joint arthroplasties and dental implants. For in vivo use, an implant made from biomaterials must have superior mechanical characteristics such as high wear resistance, hardness, and fracture toughness. For example, in joint replacements, these characteristics are especially important because joints have complex shapes and are subjected to severe external forces such as cyclic rubbing and impact. Artificial joints are generally made from a combination of titanium alloys, cobalt-chromium alloys, and ultra-high-molecular-weight polyethylene, which are used for the fixture, sliding part for hard surfaces, and sliding part for soft surfaces, respectively. Biomaterials with high wear resistance, hardness, and fracture toughness need to be developed. Ceramics and metals generally exhibit contrasting mechanical properties: ceramics exhibit low fracture toughness and high wear resistance, while metallic materials exhibit high fracture toughness and low wear resistance. If biocompatible metals and ceramics are combined, materials with ideal properties can potentially be made.

Much research has been conducted on the fabrication and mechanical characterization of composites consisting of ceramics and metals. For example, Ahlhelm et al. [1] proposed new techniques combining tape casting, lithography-based ceramic manufacturing, and freeze foaming to produce porous or dense ceramic and ceramic-metal composites, and applied to fabrication of zirconia-steel composites for biomedical applications. They successfully fabricated the composites with both characteristics of ceramic and metal phases. Dittmer et al. [2] also developed a new technique related to high-temperature co-fired ceramic technique and fabricated cermet-ceramic composites with electrically conductive channels in an insulating ceramic matrix. These composites exhibit the characteristics of both phases, and are expected for medical application. Functionally graded materials (FGMs), in which metals and ceramics are placed on the inside and surface of the implants, respectively,

have been also attracted because desired characteristics can be derived by highly controlling the material composition in FGMs. Akmal et al. [3] fabricated stainless steel-hydroxyapatite FGMs, and investigate the biocompatibility of the FGMs. Li et al. [4] and Omidi et al. [5,6] fabricated pure titanium (Ti)-SiC FGMs and Ti-hydroxyapatite FGMs, respectively, and they examined the mechanical properties of the FGMs. These FGMs were successfully fabricated without any large voids, and exhibited the properties of both the ceramics and base metals. Recently, much attention has been paid to Ti and zirconia (especially partially stabilized zirconia, PSZ), because Ti exhibits high strength and fracture toughness and PSZ exhibits fracture toughness that is high among common ceramics, as well as hardness and wear resistance. Han et al. [7] fabricated a zirconia particulate-reinforced Ti-matrix composite by powder metallurgy. The influence of sintering temperature on compressive strength was evaluated, and the strength was found to increase with the increase of sintering temperature due to the composite becoming denser. Fernandez-Garcia et al. [8] fabricated zirconia-Ti composites by the spark plasma sintering (SPS) technique, in which the fracture toughness and strength decreased with the increase of Ti content. Tsukamoto [9] fabricated zirconia-Ti composites and FGMs via SPS. The strength of the composites was found to increase with the increase of zirconia content up to 1%, but then decreased with further increases in zirconia content. Fernandez-Garcia et al. [10] also fabricated zirconia-Ti composites and evaluated the influence of surface air-plasma treatment on hardness. We have also fabricated PSZ-Ti composites [11,12] and FGMs [13], and found that the fracture toughness of the composites and FGMs could not be improved. According to the sintering process investigated by Fukui et al. [14] and the diffusion of elements in the composites analyzed by Shinohara et al. [15], the metallic Ti phase is lost in the composites due to Ti oxide formation during sintering, and thus their fracture toughness could not be improved. If the Ti oxide formation could be suppressed and the metallic Ti phase remains in the composites, it is expected that the composites would behave in a

ductile manner. Fernandez-Garcia et al. [16] proposed a technique to fabricate a yttria coating on Ti particles using a sol-gel process for use as a starting material for sintering. They successfully suppressed the formation of Ti oxide during sintering and were able to fabricate a zirconia-Ti composite (75% zirconia and 25% Ti) with high strength. To fabricate PSZ-Ti FGMs without any reaction phases, composites must be fabricated in the full range of Ti contents under the same sintering conditions, to successfully form a graded layer. Hence, the applicability of yttria-coated Ti (cTi) and PSZ powders for fabricating composites should be investigated.

This study aims to fabricate PSZ-Ti composites to produce ceramic-metal composites without any reaction compounds, as a first step in fabricating an FGM. The sol-gel technique was applied to coat Ti particles with yttria, and cTi powder was fabricated. Then, the PSZ and cTi powders were mixed in various volume fractions and composites were fabricated via SPS. Microstructural observation and XRD analysis were performed to investigate the sintering state of the composites. Then, hardness tests and three-point bend tests were performed, and the mechanical properties were examined.

2. Experimental procedure

2.1 Raw materials

The starting powders were pure titanium (Ti, Toho Titanium Co. Ltd.) and partially stabilized zirconia (ZrO_2-3molY_2O_3, PSZ, KCM Corporation Co. Ltd.). Tables 1 and 2 show the chemical composition and average diameter of the as-received powders, respectively. The values in these tables are representative obtained from the suppliers. Each as-received powder was milled using a vibrational ball milling apparatus (Nissin Giken Co. Ltd.) for 7 h in vacuum (several tens of Pa) to deagglomerate the powder. Figure 1 shows micrographs of the milled powders observed by scanning electron microscopy (SEM, VE-9800, Keyence Co.).

Table 1 Chemical composition of raw powders (mass%). (a) Ti powder and (b) PSZ powder.

(a)

Fe	Si	Mn	Cl	C	N	O	H	Ti
0.03	<0.01	<0.01	0.002	<0.01	0.02	0.19	0.03	Bal.

(b)

ZrO_2	Y_2O_3	SiO_2	Al_2O_3	Fe_2O_3
94.30	5.35	0.0122	0.2325	0.0009

Table 2 Average diameter of as-received raw powders (μm).

Ti	PSZ
23	0.35

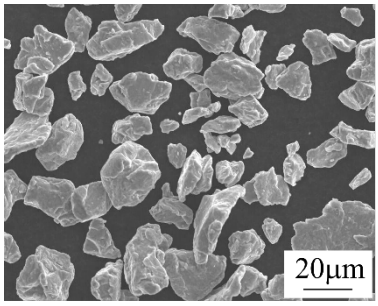

(a)

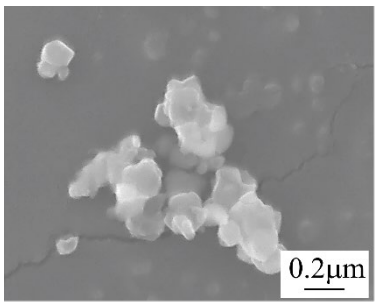

(b)

Fig. 1 Microstructure of milled powders. (a) Ti powder and (b) PSZ powder.

2.2 Fabrication of yttria-coated Ti powder by sol-gel process

In this study, the sol-gel technique proposed by Fernandez-Garcia et al. [16] was applied to form a yttria (Y_2O_3) coating on Ti powder. Yttrium chloride hexahydrate ($YCl_3 \cdot 6H_2O$, Fujifilm Wako Pure Chemical Corporation) of 0.4 g was dissolved in deionized water, and the Ti powder of 10 g was placed into the solution. The solution was stirred at 200 rpm and 80 °C using a hot-plate stirrer apparatus (Corning PC-450D, Taitec Corporation), and ammonium hydroxide (NH_4OH, Fujifilm Wako Pure Chemical Corporation) was added into the solution in a dropwise manner until the solution was gelled. Then, the gel was dried at 200 °C for 1 h, and the powder product was obtained. Finally, the powder was heated at 700 °C for 1 h in vacuum to remove impurities such as chloride.

To investigate the coating formation, the cross-section of a coated Ti particle was observed using an electron probe micro-analyzer (EPMA, JXA-8530F, JEOL Ltd.). Figure 2(a), (b), and (c) show the SEM image, elemental mapping of Ti, Y, and O, and element concentration distributions at the centerline of a Ti particle, respectively. The element concentration distributions were determined based on a simplified analysis using the collected spectra. Note that the element O was detected outside the particle, because the particle was embedded in epoxy resin to cut the particle in half. It was confirmed that Y surrounded the Ti particle thinly, and the thickness of the Y_2O_3 coating was approximately 3 μm. Additionally, Y_2O_3 powder without Ti was also detected. The sol-gel process produced both cTi and Y_2O_3 powders. It was impossible to separate only the cTi powder, and the mixed powders of cTi and Y_2O_3 were used for sintering as a starting material.

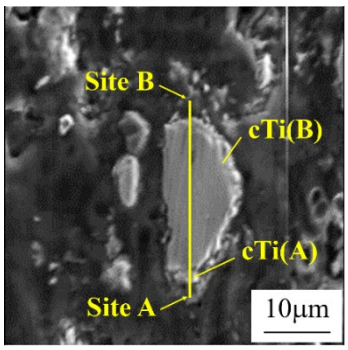

(a)

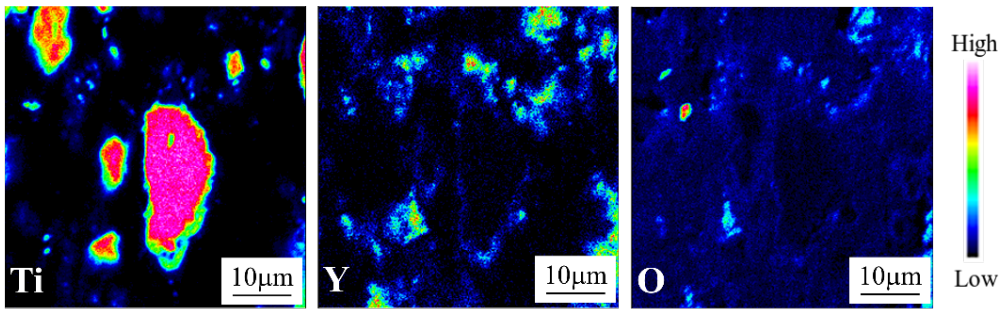

(b)

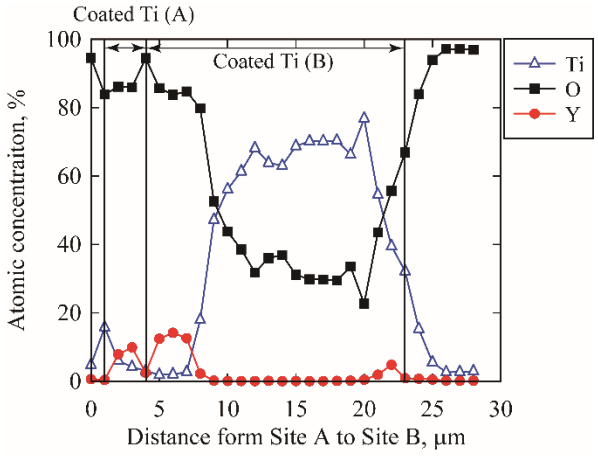

(c)

Fig. 2 Cross-sectional observations of Y_2O_3 coating. (a) SEM image, (b) elemental mapping of Ti, Y, and O, and (c) element concentration distributions at the center line of a Ti particle.

2.3 Sintering of PSZ-cTi composites

The powders of PSZ and cTi were mixed in various volume ratios from 100% cTi to 100% PSZ at 25% intervals by vibrational ball milling, under the same conditions described in Sec. 2.1. In this study, the amount of cTi was regarded as the amount of Ti. The mixed powders were placed in a graphite die with an inner diameter of 10.5 mm and a plunger of diameter 10 mm. Then, the mixed powders were sintered under uniaxial pressure of 100 MPa at 1300 °C in vacuum using an SPS apparatus (SPS-211Lx, Fuji Electronic Industrial Co. Ltd.). The heating program was as follows: heating at 300 °C/min below 600 °C, 200 °C/min from 600 to 1000 °C, 100 °C/min over 1000 °C, holding for 30 min at 1300 °C, followed by cooling at 50 °C/min. In the sintering process, the temperature at the die surface was measured by an infrared pyrometer (IR-AHS, CHINO Corp.), and the temperature was controlled at the die surface. The sintering condition for densification was preliminarily determined by trial and error. Note that it was not an objective of the present study to find an optimum sintering condition for each composite. The specimens are referred to by their Ti content, except for the monolithic PSZ specimen: 100%cTi, 75%cTi, 50%cTi, 25%cTi, and 100%PSZ.

Figures 3(a) and (b) show temperature and plunger displacement as functions of time for the monolithic cTi (100%cTi) and monolithic Ti (100%Ti), respectively. For investigation of the influence of the Y_2O_3 coating on sintering, the relationship of monolithic Ti (100%Ti) previously fabricated is shown in Fig. 3(b) [12]. Note that the sintering condition used for 100%cTi is different from that for 100%Ti because 100%cTi exhibited low sinterability compared with 100%Ti, from our preliminary investigation. According to the displacement changes, the densification of 100%cTi finished at 1200 °C in the heating process, while the densification of 100%Ti was finished at 1000 °C in the heating process.

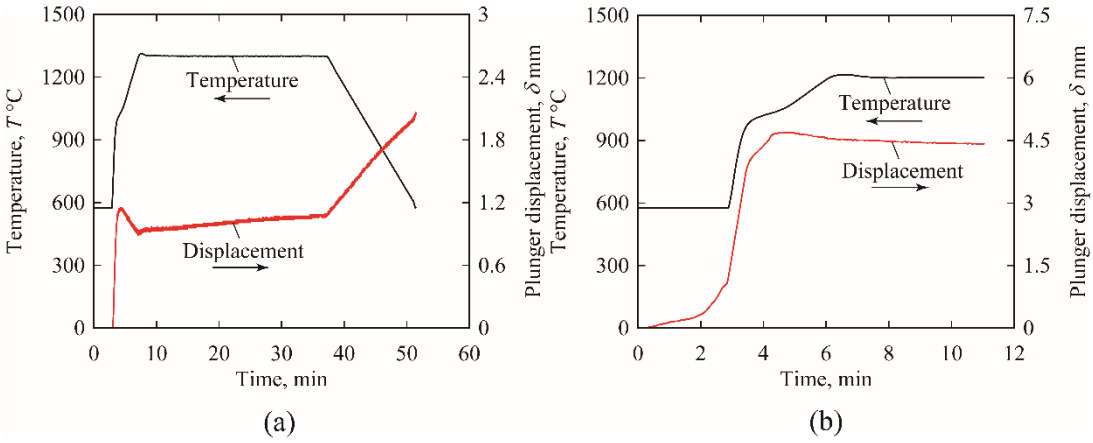

Fig. 3 Temperature and plunger displacement as functions of time. (a) 100%cTi and (b) 100%Ti

Figure 4 shows the relationship among temperature, plunger displacement, and the time for monolithic PSZ (100%PSZ), and Figure 5(a) and (b) show the relationship among temperature, plunger displacement, and time for the cTi-rich composite (75%cTi) and PSZ-rich composite (25%cTi), respectively. The densification of 100%PSZ finished at 1200 °C in the heating process, and the densification behavior of the composites tended to be intermediate between those of 100%cTi and 100%PSZ. After sintering, sintered compacts (composites) of ϕ10 × 5 mm were obtained.

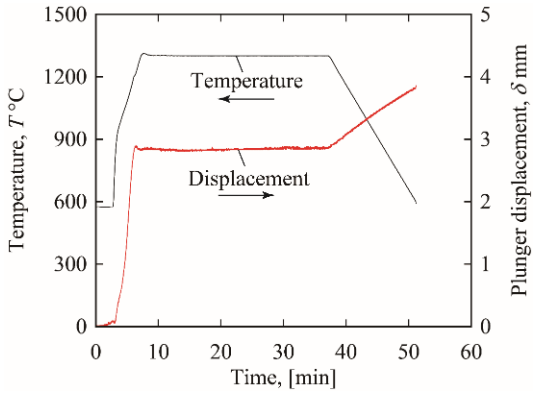

Fig. 4 Temperature and plunger displacement as functions of time for 100%PSZ.

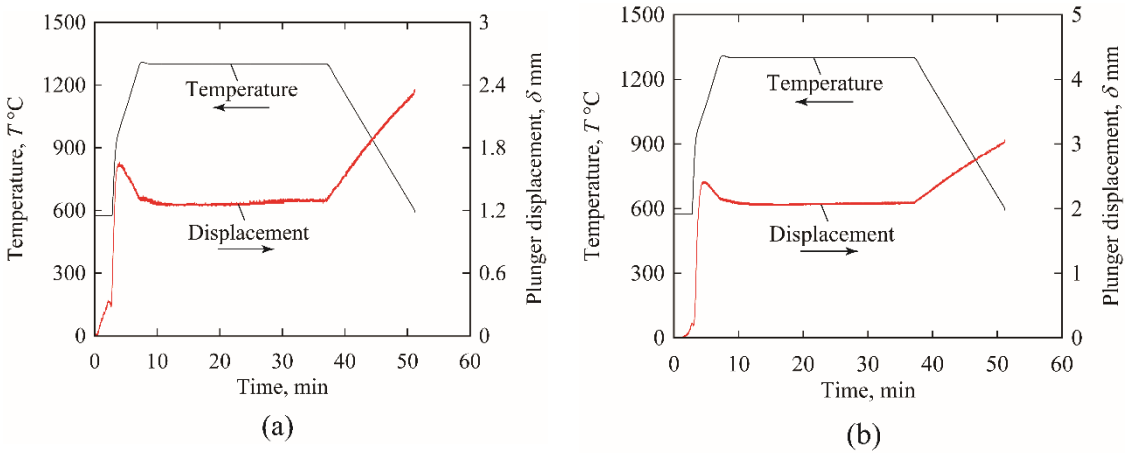

Fig. 5 Temperature and plunger displacement as functions of time. (a) 75cTi and (b) 25%cTi.

2.4 Sintering state of PSZ-cTi composites

The sintered compacts were cut in half, and their cross-sections were ground and polished with grit sandpaper and diamond paste with an average grain size of 0.25 μm, respectively. Each cross-section was observed by optical microscopy (Olympus Corp., GX51). Then, X-ray diffraction (XRD) analysis was conducted using a Cu target at an accelerating voltage of 40 kV and a current of 40 mA using an XRD apparatus (Rint Ultima II, Rigaku Corporation). The peaks in each XRD pattern were compared with Powder Diffraction File (PDF) data (PC-PDF, 1999), and the phases were identified, including sintering reaction products.

2.5 Bend testing and indentation testing

Three-point bend tests were performed using smooth rectangular specimens with a height of 2 mm, a width of 2 mm, and a length of around 10 mm using a precision universal tester (AGS-X 5kN, Shimadzu Co.). Two specimens for each composite were tested at a crosshead speed of 0.1 mm/min at room temperature. The

relationship between load and strain at the tensile side was measured with a strain gauge (FLKB-1-11, gauge length 1.0 mm, Tokyo Measuring Instruments Laboratory Co, Ltd.). The bending stress σ_b was calculated by,

$$\sigma_b = \frac{3PS}{2bh^2}, \qquad (1)$$

where *P*, *S, b*, and *h* are the load, span (8 mm), width, and height, respectively. Based on the stress-strain curve, the elastic modulus and bending strength were determined. Then, the fracture surfaces were observed with an SEM (VE-9800, Keyence Co.).

Vickers hardness testing was performed using a micro-Vickers hardness tester (MVK-E, Akashi Co. Ltd.). Ten trials for each composite were conducted under an applied load of 9.8 N at a holding time of 30 s at room temperature. The Vickers hardness was calculated by

$$HV = 0.001854\frac{F}{d^2}, \qquad (2)$$

where *F* is the indentation force (N) and *d* is the indentation diagonal length (mm).

Cracks were initiated at the corners of the indentation for 100%PSZ, 75%cTi, and 50%cT. When the average half-crack length *C* was 2.5 times larger than the average half-diagonal indent length *a*, the fracture toughness was obtained by the IF method based on JIS R 1607 (Japanese Industrial Standard) [17],

$$K_C = 0.026\frac{E^{\frac{1}{2}}F^{\frac{1}{2}}a}{C^{\frac{1}{2}}} \text{ for } \frac{C}{a} > 2.5, \qquad (3)$$

where *E* is the elastic modulus of the specimen. When the above conditions were not satisfied, fracture toughness was obtained by the Palmqvist method demonstrated by Niihara et al. [18],

$$K_C = 0.035\left(\frac{C-a}{a}\right)^{-0.5}\left(\frac{HV\phi}{a^{0.5}}\right)\left(\frac{HV}{\phi E}\right)^{-0.4}, \qquad (4)$$

where ϕ is the ratio of hardness and yield stress and is set at 3 in this study as an approximation used by Li et al. [19]. The average fracture toughness of each composite was obtained from five trials.

3. Experimental results and discussion

3.1 Microstructure and sintering state of alumina-PSZ composites

Figure 6 shows the microstructure of the composites. For 100%cTi, the Ti and Y_2O_3 phases were well dispersed with no large voids, and it appeared that 100%cTi was fabricated as a Ti-Y_2O_3 composite. As for 100%PSZ, no large voids were observed. For the composites, the Ti, Y_2O_3, and PSZ phases were well dispersed in all composites, although PSZ aggregation was partially observed.

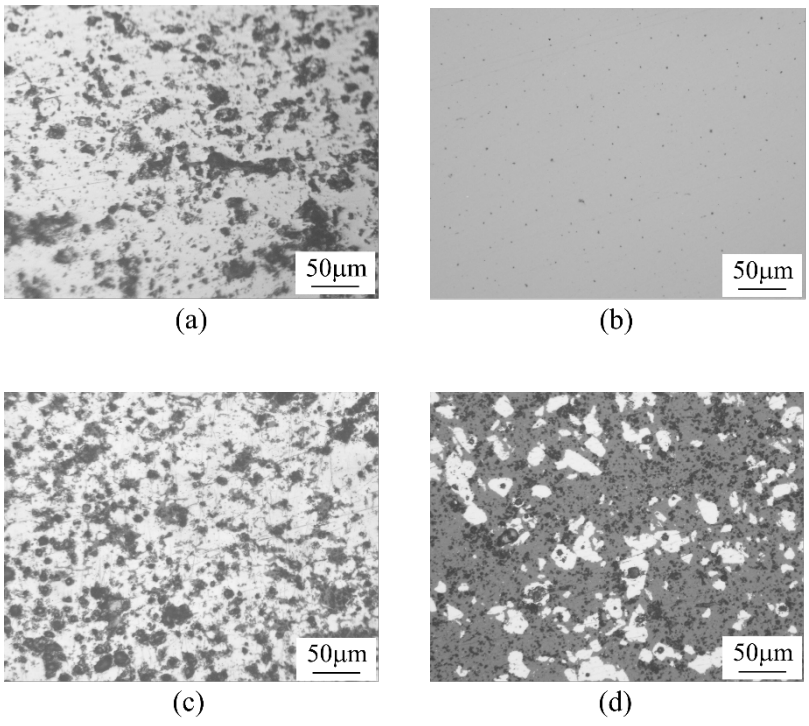

Fig. 6 Optical microscopy observations. (a) 100%cTi, (b) 100%PSZ, (c) 75%cTi, and (d) 25%cTi.

Figure 7 (a) and (b) shows the XRD patterns of PSZ-cTi and PSZ-Ti composites, respectively. Only the phases of Ti, Y_2O_3, and ZrO_2 were identified in PSZ-cTi composites, while some reaction products of Ti_2O and Ti_2ZrO in addition to the phases of Ti, Y_2O_3, and ZrO_2 were detected in the PSZ-Ti composites. Based on the comparison of the phases in these composites, it was inferred that the Y_2O_3 coating acted as a barrier and prevented Ti oxidation caused by diffusion of oxygen from the PSZ phase to the Ti phase during sintering. Hence, the presence of a ceramic coating on the starting metallic powder is effective for the suppression of oxygen diffusion and metal oxide formation during sintering.

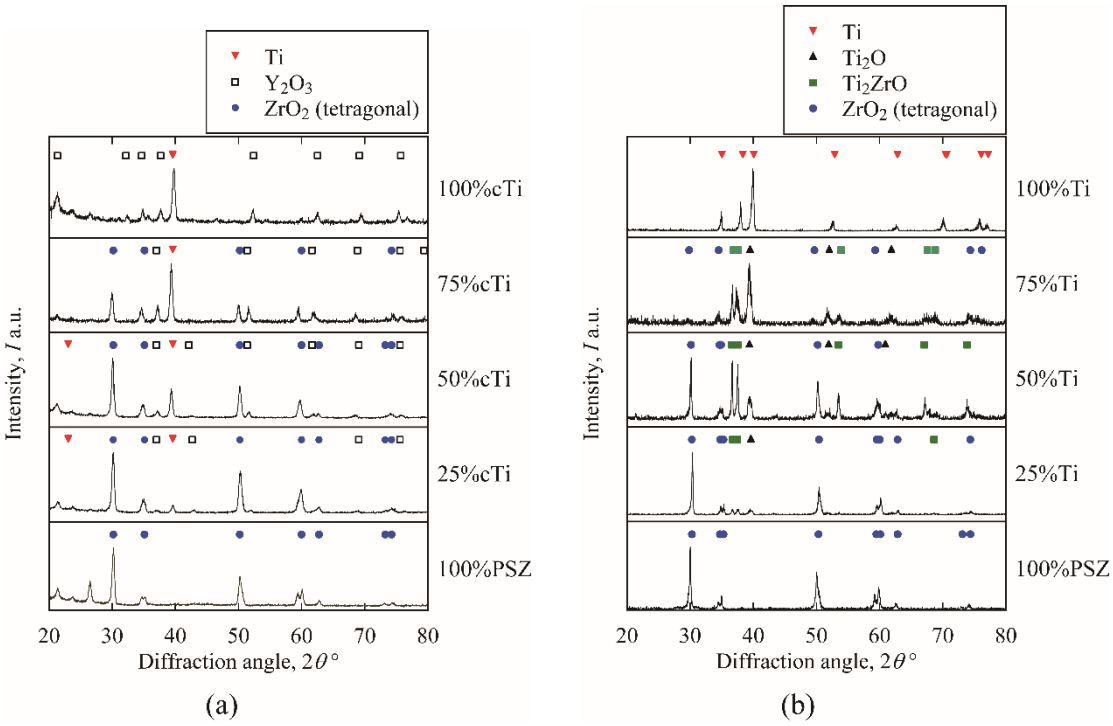

Fig. 7 XRD patterns. (a) PSZ-cTi composites and (b) PSZ-Ti composites.

3.2 Bending properties of PSZ-cTi composites

Figure 8 shows typical stress-strain curves of the composites. Brittle fracture occurred with little plastic deformation for the composites, 100%PSZ, and 100%cTi.

Even though 100%cTi was fabricated, the ductility of the pure Ti phase appeared to have been lost with the dispersion of the Y_2O_3 phase. The mechanical properties of elastic modulus and bending strength were obtained from these curves.

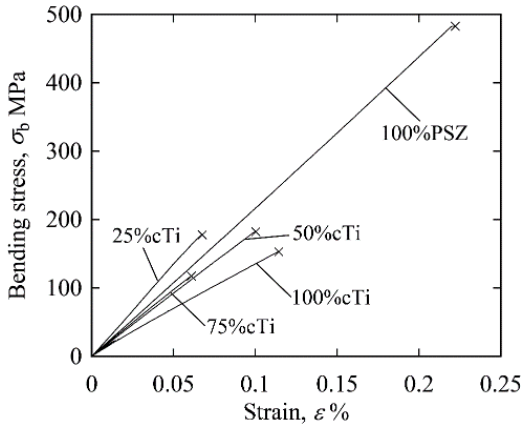

Fig. 8 Bending stress-strain curves.

Figure 9 shows the elastic modulus of the PSZ-cTi and PSZ-Ti composites as a function of cTi/Ti content. The scatter bars denote the maximum and minimum values of two specimens for each composite. Their elastic modulus decreased with the increase of cTi content. The dotted line denotes the prediction based on the rule of mixture, which agrees relatively well with the experimental results. The relationship between elastic modulus and PSZ content in the PSZ-Ti composites along with the values based on the rule of mixture is also drawn in Fig. 9. The elastic modulus of each composite is higher than the predicted value. These results can be explained based on the phases being present in the composites. From Fig. 7, the PSZ-cTi composites consist of only Ti, Y_2O_3, and PSZ phases, and the elastic modulus of the composites is comparable to the prediction based on the rule of mixture. On the other hand, the PSZ-Ti composites consist of Ti, PSZ, and other reaction phases with high elastic modulus, and the elastic modulus of the composites becomes high due to the reaction phases. The relationship between reaction phases and elastic modulus was discussed in detail by Fujii et al. [11].

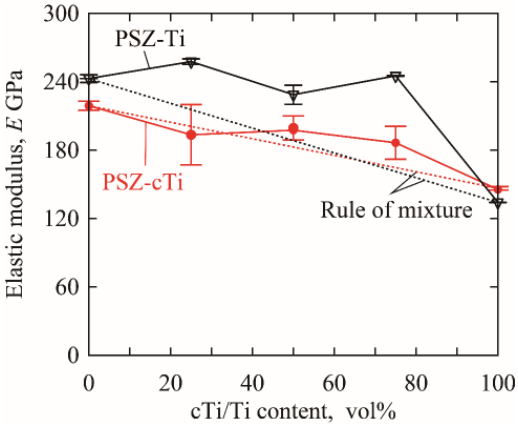

Fig. 9 Elastic modulus as a function of cTi/Ti.

Figure 10 shows the bending strength of the PSZ-cTi and PSZ-Ti composites as a function of cTi/Ti content. The scatter bars denote the maximum and minimum values of two specimens for each composition. The bending strength of the PSZ-cTi composites was low, irrespective of cTi content, compared with 100%PSZ. Moreover, the bending strength of the PSZ-cTi composites was also lower than that of the PSZ-Ti composites. To investigate the reason for the reduction in the strength of PSZ-cTi composites, their fracture surfaces were observed, as shown in Fig. 11. Cleavage fracture in the Y_2O_3 phase and/or intergranular fracture was observed for all composites, including 100%cTi. Gan et al. [20] pointed out that the bending strength of Y_2O_3 ceramic is quite low, compared with PSZ and Ti. Hence, the strength of the PSZ-cTi composites became low, compared with the PSZ-Ti composites. The presence of the Y_2O_3 phase had a positive effect on elastic behavior and a negative effect on fracture behavior. Note that the bending strength of 100%PSZ fabricated in this study was also lower than that of 100%PSZ in the previous study. This would be due to the grain size effect. Stawarczyk et al. [21] pointed out that the grain size of zirconia increased with increasing sintering temperature. It is well known that the strength of polycrystalline ceramics increases with decreasing grain size of the ceramics [22-24]. Comparing the

325 sintering conditions of these studies, the sintering temperature in this study was higher
326 than that in the previous study. As a result, the grain size of 100%PSZ fabricated in this
327 study would be larger than that of 100%PSZ fabricated in the previous study, although
328 the grain size of 100%cTi and 100%Ti could not be measured. Hence, it was considered
329 that the difference in strength was caused by the difference in grain size resulting from
330 the different sintering temperatures.

331

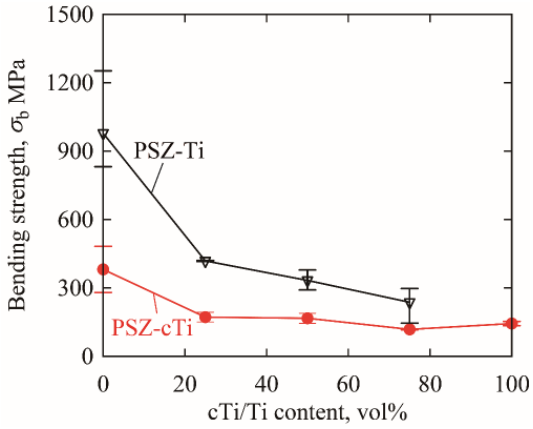

332 Fig. 10 Bending strength as a function of cTi/Ti.

333

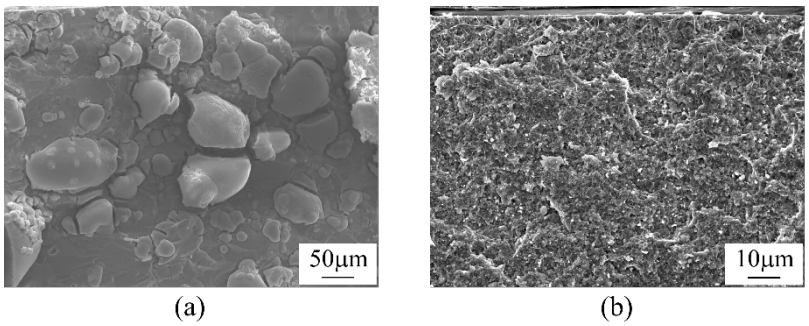

334

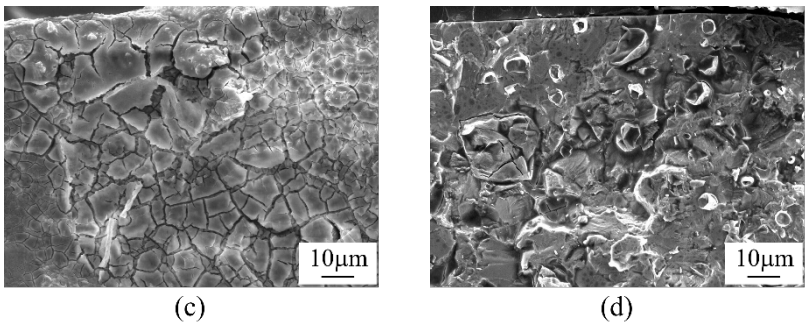

335 Fig. 11 Fracture surfaces. (a) 100%cTi, (b) 100%PSZ, (c) 75%cTi, and (d) 25%cTi.

3.3 Hardness and fracture toughness of PSZ-cTi composites

Figure 12 shows the relationship between Vickers hardness *HV* and PSZ content in the PSZ-cTi and PSZ-Ti composites. The scatter bars denote the maximum and minimum hardness of five trials for each composition, and the dotted lines denote the prediction by the rule of mixture. The hardness of the composites decreased with the increase of cTi content in the PSZ-cTi composites and agreed with the prediction. On the other hand, the hardness of the PSZ-Ti composites was much higher than predicted. This is because the PSZ-cTi composites consist of only Ti, Y_2O_3, and PSZ phases while the PSZ-Ti composites consist of Ti, PSZ, and other phases with high hardness, as mentioned in Sec. 3.2.

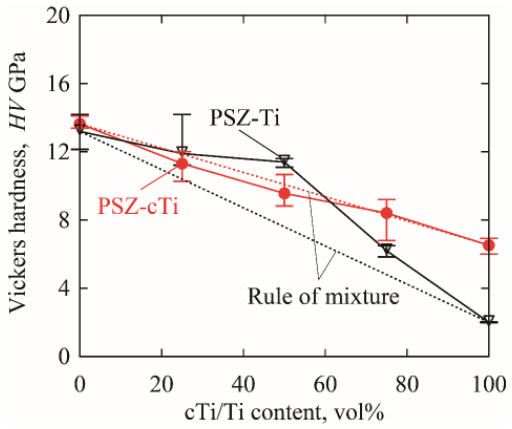

Fig. 12 Hardness as a function of cTi/Ti.

Figure 13 shows the relationship between fracture toughness K_C and PSZ content in the PSZ-cTi and PSZ-Ti composites. The scatter bars denote the maximum and minimum hardness of five trials for each composition. Note that no cracks occurred in 75%cTi and 100%cTi, and the fracture toughness could not be measured. The fracture toughness K_C decreased with the increase of cTi/Ti content in both composites. As for the PSZ-Ti composites, they consisted of brittle PSZ, Ti oxide, and reaction

products without ductile Ti, so that the fracture toughness could not be improved. On the other hand, for the PSZ-cTi composites, the metallic Ti phase, which was ductile, remained in the composites. However, according to Fig. 11(c), brittle fracture in the Y_2O_3 phase around the Ti phase was observed in the PSZ-cTi composites. It was expected that cracks from the indentation corners also occurred along the brittle Y_2O_3 phase, and hence the fracture toughness could not be improved. As for 75%cTi and 100%cTi, the fracture toughness could not be measured, but their fracture toughness would be expected to be low, considering their stress-strain curves.

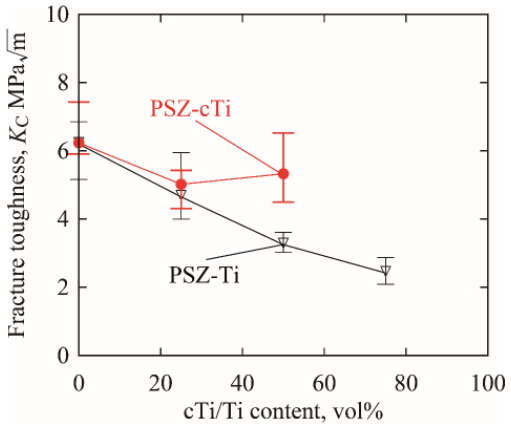

Fig. 13 Fracture toughness as a function of cTi/Ti.

In this study, the use of Y_2O_3-coated Ti powder as a starting material could suppress sintering reactions, such as oxidation of the Ti phase. As a result, the hardness and elastic modulus of the composites agreed with the prediction of the rule of mixtures, and the composites exhibited low strength and brittleness due to the brittle Y_2O_3 phase. There are few structural materials that can be used as implant materials, and both PSZ and Ti are still attractive materials. As it was possible to suppress Ti oxidation during sintering in this study, the improvement of the strength and fracture toughness of these composites will further investigated from a microstructural viewpoint.

4. Conclusions

To fabricate PSZ-Ti composites having ceramic and metallic characteristics, the powders of Y_2O_3-coated Ti (cTi) and PSZ was used, and the PSZ-Ti composites containing the Y_2O_3 phase (PSZ-cTi composites) were fabricated via SPS ranging from pure cTi to pure PSZ. The obtained results are summarized as follows:

(1) The Y_2O_3 coating with approximately 3 μm thick on Ti powder was formed by the sol-gel process.

(2) The dense PSZ-cTi composites were fabricated in the full range of cTi contents under the conditions of sintering temperature 1300 °C, uniaxial pressure of 15 MPa, and holding time of 30 min.

(3) Chemical reactions did not occur during sintering, based on the XRD analysis. The Y_2O_3 coating on Ti powder acted as a barrier and prevented Ti oxidation caused by oxygen diffusion during sintering.

(4) The elastic modulus and hardness of the composites decreased with the increase of cTi content and agreed with the prediction of the rule of mixtures. The bending strength and fracture toughness of the composites could not be improved because the fracture occurred along the weak Y_2O_3 phase, irrespective of cTi content.

References

[1] M. Ahlhelm, P. Gunther, U. Scheithauer, E. Schwarzer, A. Gunther, T. Slawik, T. Moritz, A. Michaelis, *J. Eur. Ceram. Soc.*, 2016, Vol. 36, pp. 2883-2888.

[2] R. Dittmer, M. Christian, J.F. Fischer, U. Hausch, J. Troetzschel, H. Specht, *Biomed. Mater.*, 2017, Vol. 75, pp. 206-211.

[3] M. Akmal, M.S. Hussain, H. Ikram, T. Sattar, S. Jameel, K.Y. Kim, F.A. Khalid, J.W. Kim, *Ceram. Int.*, 2016, Vol. 42, pp. 3855-3863.

[4] S.N. Li, H.P. Xiong, N. Li, B.Q. Chen, C. Gao, W.J. Zou, H.S. Ren, *Ceram. Int.*, 2017, Vol. 43, pp. 961-967.

[5] N. Omidi, A.H. Jabbari, M. Sedighi, *Powder. Metall.*, 2018, Vol. 61, pp. 417-427.

[6] M. Sedighi, N. Omidi, A. Jabbari, *Mech. Adv. Compos. Struct.*, 2017, Vol. 4, pp. 233-237.

[7] C. Han, Y. Li, X. Lian, L. Chen, N. Zhao, X. Zhu, *Trans. Nonferrous Met. Soc. China*, 2012, Vol. 22, pp. 1855-1859.

[8] E. Fernandez-Garcia, C.F. Gutierrez-Gonzalez, A. Fernandez, R. Torrecillas, S. Lopez-Esteban, *Ceram. Int.*, 2013, Vol. 39, pp. 6931-6936.

[9] H. Tukamoto, *Int. J. Mater. Sci. Appl.*, 2014, Vol. 3, pp. 260-267

[10] E. Fernandez-Garcia, X. Chen, C.F. Gutierrez-Gonzalez, A. Fernandez, S. Lopez-Estebanc, C. Aparicio, *J. Dent.*, 2015, Vol. 43, pp. 1162-1174.

[11] T. Fujii, K. Tohgo, H. Araki, K. Wakazono, M. Ishikura, Y. Shimamura, *J. Solid Mech. Mater. Eng.*, 2010, Vol. 4, pp. 1699-1710.

[12] K. Tohgo, T. Fujii, M. Harada, H. Isono, Y. Shimamura, *Mat. Sci. Eng. A-Struct.*, 2015, Vol. 621, pp. 166-172.

[13] T. Fujii, K. Tohgo, H. Isono, Y. Shimamura, *Mat. Sci. Eng. A-Struct.*, 2017, Vol. 682, pp. 656-663.

[14] Y. Fukui, T. Fujii, K. Tohgo, Y. Shimamura, *Comp. Mater. Sci*, 2014, Vol. 95, pp. 24-34.

[15] T. Shinohara, T. Fujii, K. Tohgo, Y.Shimamura, *Mater. Char.*, 2017, Vol. 132, pp. 230-238.

[16] E. Fernandez-Garcia, C.F. Gutierrez-Gonzalez, P. Peretyagin, W. Solis, S. Lopez-Esteban, R. Torrecillas, A. Fernandez, *Mat. Sci. Eng. A-Struct.*, 2015, Vol. 646, pp. 96-100.

[17] Japanese Industrial Standard, JIS R 1607, 2015.

[18] K. Niihara, R. Morena, D.P.H. Hasselman, *J. Mater. Sci. Lett.*, 1982, Vol. 1, pp. 13-16.

[19] Z. Li, A. Ghosh, A.S. Kobayashi, R.C. Bradt, *J. Amer. Ceram. Soc.*, 1989, Vol. 72, pp. 904-911.

[20] L. Gan, Y.J. Park, L.L. Zhu, H.N. Kim, J.W. Ko, H.D. Kim, *J. Eur. Ceram. Soc.*, 2018, Vol. 38, pp. 4064-4069.

[21] B. Stawarczyk, M. Özcan, L. Hallmann, A. Ender, A. Mehl, C.H.F. Hämmerlet, *Clin Oral Invest,* 2013, Vol. 17**, pp.** 269–274.

[22] F.P. Knudsen, *J. Amer. Ceram. Soc.*, 1959, Vol. 42, pp. 376-387.

[23] S.C. Carniglia, *J. Amer. Ceram. Soc.*, 1965, Vol. 48, pp. 580-583.

[24] W.D. Kingery, H.K. Bowen, D.R. Uhlmann, *Introduction to Ceramics*, 2nd ed., John Wiley and Sons, New York, NY, 1976, p. 768.